



# Study on Microstructure and Thermal Cycling Performance of the Plasma-sprayed YSZ Coating in Simulated Turbine Environment

S. M. Muthu<sup>1</sup> · M. Arivarasu<sup>2</sup> · Changheui Jang<sup>1</sup> · S. Viknesh<sup>3</sup> ·  
K. Surya Prakash Reddy<sup>4</sup> · M. Venkateshkannan<sup>5</sup> · V. D. Vishnu Siddharth<sup>4</sup> ·  
Nafeez Ahmed Liyakat<sup>6</sup>

Received: 19 April 2023 / Revised: 13 July 2023 / Accepted: 14 July 2023 /  
Published online: 31 July 2023

© The Author(s), under exclusive licence to Springer Science+Business Media, LLC, part of Springer Nature 2023

## Abstract

To enhance the efficiency and durability of the gas turbine and aircraft components, thermal barrier coatings (TBCs) are the most considerable protection techniques available. The present work is mainly concentrating on improving the high-temperature corrosion characteristics of uncoated and plasma-spray coated alloy A-286 under  $\text{Na}_2\text{SO}_4$ -5%NaCl-7.5%NaVO<sub>3</sub> deposit at 900°C. By using plasma spray process NiCrAlY and YSZ (bond coat-NiCrAlY and top coat-YSZ) thermal barrier coating was deposited on the alloy A-286. Coating characterization such as roughness was analysed on the coating surface and coating thickness and hardness analysis were performed on the coating region at the cross section. X-ray diffraction (XRD) and scanning electron microscope (SEM) were employed to study the phases and coating microstructure before and after being subjected to corrosion. The rate of corrosion was derived by thermo-gravimetric analysis. Using the elemental mapping technique and EDS compositional analysis, the scale thickness and corrosion attack were identified. During the corrosion experiment, sputtering and spallation of oxide were noticed on the uncoated specimen. The oxide layer failure was not found in both the coated specimens. The results indicated that YSZ coating exhibits a better corrosion resistance than NiCrAlY. The reaction products such as monoclinic ZrO<sub>2</sub> and YVO<sub>4</sub> were found in the corroded YSZ coating. There was no significant failure, but degradation was found on the coating due to molten salt.

**Keywords** Alloy A-286 · Thermal barrier coating · Plasma spray coating · High temperature corrosion · Thermogravimetric analysis · Reaction products

## Introduction

A-286 alloy is a precipitation-hardenable Fe-based alloy (strengthening phase  $\text{Ni}_3(\text{Al}, \text{Ti})$ ) and has an austenitic structure. It is extensively used in various industrial sectors such as in aerospace, jet engines, gas turbine blades, rotors, afterburners and acidic environments like chlorine, sulfuric acid and for the superior hydrogen use environment because of its good mechanical strength, thermal resistance and enormous corrosion resistance. This alloy is mainly used in the joining surface of gas turbines where surfaces like power turbine inlets and gas turbines exit. In the gas turbine environment, the alloy is more susceptible to corrosion attack [1–3]. The major issue in high temperature gas turbine industries is hot corrosion due to oxidation and salt deposition at high temperatures. The fuels used in the aero engine and gas turbine industries contain corrosive elements such as vanadium, sodium and sulphur. At elevated temperatures, these corrosive elements get oxidized and react with one another resulted in the formation of  $\text{Na}_2\text{SO}_4$ ,  $\text{NaVO}_3$  and  $\text{V}_2\text{O}_5$ , etc. These corrosive species could deposit on the hot section of the parts, which results in deterioration of the metals and later it leads to the failure of the components. The failure of these components results in damage to the physical and chemical properties. In order to protect these hot parts from high temperature as well as salt, it is significant that the samples should be coated with corrosion-resistant metallic and ceramic materials using thermal spray coating techniques [3–6].

Generally, thermal spray coatings like plasma spray, cold spray, high-velocity oxy-fuel and plasma spray-physical vapour deposition are widely encouraged for protecting the parts when exposed to high temperature. The various coating materials such as  $\text{Cr}_3\text{C}_2$ -25%NiCr,  $\text{Ni}_3\text{Al}$ , Ni-20%Cr, NiCrAlY, and YSZ were widely prepared by different thermal spray procedures for enhancing hot corrosion and oxidation resistance [6, 7]. In this decade, to prevent the hot section parts in gas turbine applications from corrosion and to increase the turbine inlet operating temperature to increase the efficiency of the engine by offering the thermal insulation properties using thermal barrier coatings (TBCs). TBC system is a combination of ceramic top coat and metallic bond coat. The metallic bond coat (BC) MCrAlY (M refers Co, Ni and Ni/Co) offers the corrosion and oxidation resistance due to the development of oxides of Ni, Al and Cr at elevated temperature and Y exhibit the adhesion behaviour between the top coat and bond coat [8–10]. The main purpose of the topcoat (TC) is to reduce the heat transfer to the substrate which is related to the thermal conductivity. Yttrium stabilized zirconia (YSZ) is widely preferred as the TC material in TBC system because of its low thermal conductivity and high thermal expansion coefficient (CTE) which is near to the substrate and coating. The thermal insulation properties provided by ceramic yttrium stabilized zirconia (YSZ) topcoat (TC) which has high thermal expansion ( $11 \times 10^{-6} \text{ }^\circ\text{C}^{-1}$ ) and is near to BC CTE value ( $14 \times 10^{-6} \text{ }^\circ\text{C}^{-1}$ ), a low thermal conductivity ( $1.2\text{--}1.8 \text{ Wm}^{-1} \text{ K}^{-1}$ ) and high strain tolerance and compliance. The TC material 7–8%YSZ acts as a thermal insulator which is made from  $\text{Y}_2\text{O}_3$  (4–4.5 mol%) stabilized  $\text{ZrO}_2$  [10–14]. When the TBC is exposed to high

temperature, an oxide layer will be generated between TC and BC which is called as thermally grown oxide (TGO). It leads to TBC failure and spallation of the TC causing compressive residual stress. In addition, thermal expansion coefficient mismatch between the BC and TC can exasperate to failure in the coating during thermal cycles. In TBC system, plasma spray is the widely employed method to prepare ceramic topcoat due to its more economic and the coating depositions are carried out at a high temperature and open atmosphere and also have unique advantages easy deposition and cost-effective [13–15]. NiCrAlY coating holds excellent corrosion resistance behaviour because of the development of protective  $\text{Cr}_2\text{O}_3$ , NiO and  $\text{Al}_2\text{O}_3$  layer. Generally, these oxide layers have a high melting point and are even stable, which provides corrosion resistance upto  $900^\circ\text{C}$  [16].

Muthu et al. [3] performed protective Ni and Cr coating on alloy A-286 using HVOF and investigated the hot corrosion characteristics of the samples in aggressive salt condition at  $700^\circ\text{C}$ . The author reported that bare metal experienced to severe corrosion attack and the coating protects the material against salt is attributed to the protective scales developed on the surface. Gurdeep et al. [17] investigated the corrosion performance on SA213-T-22 steel with plasma-coated  $\text{Al}_2\text{O}_3\text{--TiO}_2$  in molten salt of sulphate and vanadate environment at  $900^\circ\text{C}$ . From the results, the author mentioned that the uncoated specimen was more prone with corrosion and gained more weight as compared to the coated specimen which forms a better protective oxide layer. The author reported that the coating employed by plasma provides protection and also rate of corrosion is highly dependent on the partial pressure of oxygen present in the atmosphere. Many researchers have suggested that plasma spray coating is the common method and best choice for TBC preparation. Lie et al. [18] deposited TBC of YSZ by plasma and laser glazing method and compared the corrosion behaviour at 700 and  $1000^\circ\text{C}$  for 4 h in  $\text{V}_2\text{O}_5$  salt environment. The author observed that net-like cracks and un-melted powders on the coating surface led to the penetration of molten salts. The laser glazed coating experienced more vertical cracks which facilitated the penetration of molten salts. Further research on vertical crack width optimization can reduce the corrosion even more. Jiaqi et al. [19] prepared NiCoCrAlY-YSZ TBC on Ni-based superalloy and investigated the isothermal oxidation behaviour at 900 and  $1000^\circ\text{C}$  and TGO growth rate. The authors reported that the pores and micro-cracks on the surface of the coating are due to volumetric shrinkage or expansion and inner oxide in the interface of bond coat and topcoat. It was inferred that the average thickness of scale and inner oxide zone was significantly smaller in the coated sample than compared to the uncoated substrate. Lakshmi et al. [20] analysed the hot corrosion resistance of plasma-sprayed YSZ/ $\text{Gd}_2\text{Zr}_2\text{O}_7$  TBC in the molten environment of  $\text{Na}_2\text{SO}_4 + \text{V}_2\text{O}_5$  at  $910^\circ\text{C}$ . The authors also mentioned that TBC showed higher thermal cyclic life. Samia et al. [21] used an air plasma spray system to fabricate YSZ TBC on Inconel 718 and CoNiCrAlY used as a bond coating. The authors studied the isothermal oxidation and solid particles erosion performance of the coating and reported that the failure of TC resulted in spallation during the oxidation test. The erosion resistance was improved by TBC topcoat. Xie et al. [22] used plasma spray method to deposit TBC YSZ coating on Inconel 738 with different environment conditions and further studied the effect of microstructure and defects. Mohamad et al. [23] studied the corrosion behaviour of

laser glazed and plasma-sprayed YSZ- $\text{Al}_2\text{O}_3$  in a 55% $\text{V}_2\text{O}_5$ -45% $\text{Na}_2\text{SO}_4$  environment at 1000°C for 30 h. Inconel 718 was sprayed with a NiCrAlY as a BC and YSZ- $\text{Al}_2\text{O}_3$  was deposited as a TC. The author mentioned that glazed and plasma-sprayed coatings showed similar corrosion mechanisms. However, plasma-sprayed coating showed a double increase in corrosion resistance than laser glazing because of a higher fraction of protective oxide layer  $\text{ZrO}_2$  in plasma spraying than laser glazing.

From the study on the literature that was gathered, there is no detailed study to enhance the corrosion characteristics of A-286 alloy using plasma-sprayed YSZ and NiCrAlY coating in 3SM condition. Therefore, our present work is concentrated on the preparation of TBC with low cost and investigated the hot-corrosion performance of the coated and uncoated alloy A-286 in  $\text{Na}_2\text{SO}_4$ -5% $\text{NaCl}$ -7.5% $\text{NaVO}_3$  salt environment of at 900°C. The surface morphology, phases of the reaction products developed on the specimens and corrosion attack depth were analysed using SEM and XRD. The kinetics of corrosion of the alloy was analysed using the weight change method.

## Experimental Procedures

### Samples Preparation and Coating Deposition

The substrate material alloy A-286 (Fe-56.2, Cr-13.6, Ni-24.1, Mo-1.18, Ti-1.99, Al-0.25, Co-0.32, Mn-1.21, V-0.15, Si-0.505, Cu-0.298 and C-0.046) is procured as a plate of 6 mm thickness and was cut into the size of 20 × 10 mm for coating preparation and corrosion study. The compositions of the alloy were ensured by optical emission spectroscopy (OES). Prior to coating deposition, the samples are polished using SiC sheets to remove grease, dirt and other impurities and followed by grit blasted with alumina particles to achieve a rough surface in the range of 7–10 μm for enhancing the adhesive characteristics of the coating material on the substrate. The samples were successfully coated with NiCrAlY and YSZ ( $\text{Y}_2\text{O}_3$ -stabilized zirconia ( $\text{ZrO}_2$ )) feedstock powders using plasma spray technique and the spraying parameters are listed in Table 1. To fabricate TBC, NiCrAlY (Ni-22%Cr-10%Al-1%Y) was used as a BC material and YSZ (8% $\text{Y}_2\text{O}_3$ -92% $\text{ZrO}_2$ ) as a top coat material to achieve better bonding. The coatings were performed on all the sides of the

**Table 1** Parameters of plasma spray coating on alloy A-286

Parameters	Bond coating	Top coating
Current (I)	520	600
Voltage (V)	60	70
$\text{H}_2$ flow rate ( $\text{L min}^{-1}$ )	5	5
Argon flow rate ( $\text{L min}^{-1}$ )	40	45
Spray distance (in mm)	100	90
Powder feed rate ( $\text{g min}^{-1}$ )	45	25

substrates to cover the entire surface of the alloy by coating materials to enhance the corrosion resistance.

### Coating Characteristics

Various characteristics such as roughness, microhardness, surface morphology, phases and thickness of the coating are evaluated. Mahr surface roughness tester was used to measure the roughness of the coatings in as-sprayed conditions. For cross-sectional analysis, the coated samples are cut into two halves, and the standard metallographic procedure is employed to obtain a mirror finish. The hardness of the coating region was measured across the cross section using Matsuzawa Vickers microhardness tester using a 25 g load applied for a 10 s holding time on each place for a regular interval of 50  $\mu\text{m}$ . Characterization techniques such as SEM and EDS are used to characterize the microstructure and elements present on the powders and coatings and phases were identified by XRD technique. The coating thickness measurement was done on the coating at cross section using SEM [24].

### Hot Corrosion Experiment

The corrosion study is conducted on the bare and YSZ coated alloy A-286 at 900°C in a mixture of aggressive  $\text{Na}_2\text{SO}_4$ -5%NaCl-7.5% $\text{NaVO}_3$  salt environment for 10 cycles. One cycle includes 10 h of heating the samples at 900°C and 30 min of cooling them at room temperature [25]. The salts are applied on the samples (3–5  $\text{mg}/\text{cm}^2$ ) while applying salt the specimen's temperature is maintained at 250°C to make sure that the salt deposits properly on the samples. Prior to corrosion study, the samples are then subjected to heating at 120°C for 2 h for removing moisture from the samples and crucibles. The samples were weighed after the end of each cycle using an electronic weighing balance (accuracy 0.0001 g) to ensure corrosion kinetics.

### Microstructural and Phase Analysis

Analysing methods such as SEM and XRD are performed on the scales developed on the specimens to investigate the morphology and phases. A cross-sectional study is used to ensure the scale thickness and corrosion attack using SEM investigation and EDS line scan analysis was performed on the scale to ensure the distribution of corrosion products. EDS analysis was done on the surface to identify the elements present on the corroded surface.

## Results

### Coating Characterization

SEM observation was made on the powder particles to examine the powder morphology of the commercially available NiCrAlY and YSZ powders used for preparing

TBC and the composition of the elements is analysed using EDS equipped with SEM which are shown in Fig. 1a and b. The SEM results reveal that NiCrAlY powders are irregular in shape and it has the highest weight percentage of Ni(59.56%), Cr(21.39%), Al(17.38%) and a small amount of Y(1.67%). The spherical shape YSZ powders are used as a topcoat material, and it has the highest weight percentage of Zr(58.94%) followed by O(33.78%) and Y(7.28%). It could be noticed from the SEM evaluation, the size of the NiCrAlY and YSZ powder particles was found in the range of 25–35  $\mu\text{m}$  and 20–40  $\mu\text{m}$ . The XRD analysis was done on the powder particles to investigate the phase compositions, and the results are reported in Fig. 2. The phases of the coatings were identified using the JCPDS software. In YSZ powder, ZrO<sub>2</sub> and Y are the phases present. In NiCrAlY powder, predominant elements such as Ni, Cr and Al are present along with Y which is found in a few peaks.

Figure 3 shows the graph of surface roughness profile obtained by Mahr surface roughness tester using centre-line average (CLA) method. The measurement is taken on the surface of the coated samples as-sprayed condition. The measurements were done at three different regions on the top surface of each coating for a span of 4-mm span and an average value was calculated. Table 2 shows the measured average roughness value (Ra) for the coatings and the Ra values were found in the NiCrAlY and YSZ coatings are 5.847 and 6.006  $\mu\text{m}$ , respectively. It can be observed that similar roughness values were obtained in both the case of coatings.

Plasma coating microstructure was analysed on the surface as-sprayed condition using SEM and is illustrated in Fig. 4a and b. It can be observed from the

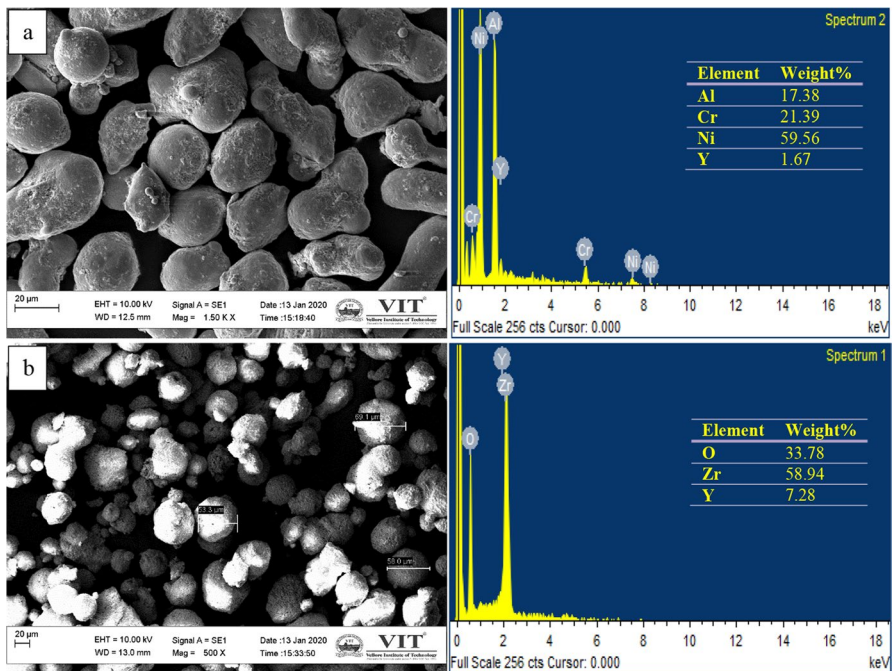
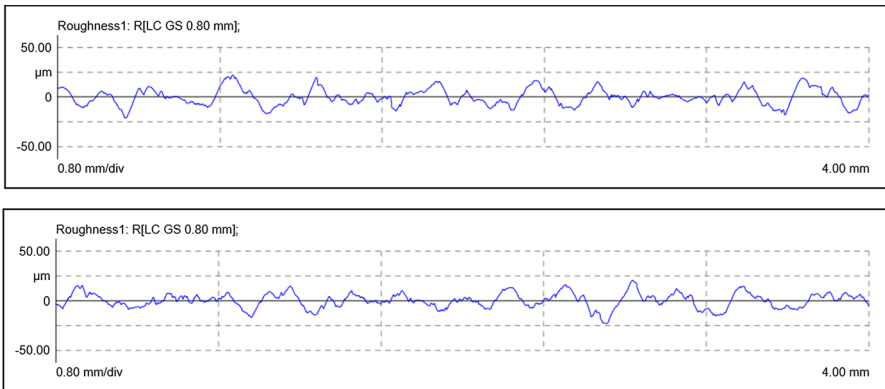
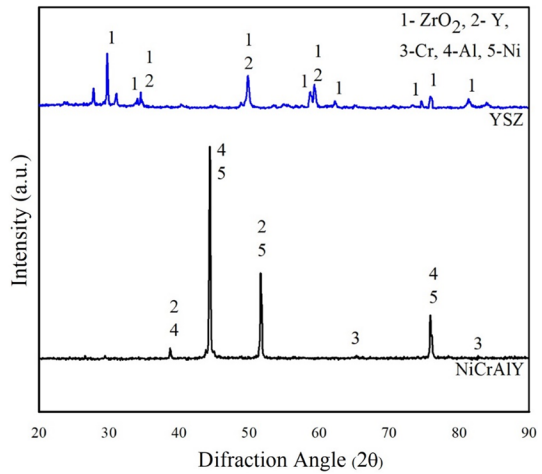


Fig. 1 SEM–EDS analysis of powder particles used for plasma spray deposition. **a** NiCrAlY and **b** YSZ

**Fig. 2** XRD analysis of powder particles used for preparation of TBC



**Fig. 3** Surface roughness profile of a NiCrAlY coating and bYSZ coating

**Table 2** Surface roughness of the plasma-sprayed coating

Coating	Ra <sub>1</sub>	Ra <sub>2</sub>	Ra <sub>3</sub>	R <sub>m</sub>
NiCrAlY	6.4575	6.0860	4.9975	5.8470
YSZ	5.7833	6.1815	6.0541	6.0063

YSZ coating, splat like structures are formed along the whole surface and show the smooth surface, whereas in NiCrAlY coating, it is seen only in a few areas. This is due to unmelted powder particles which are present due to insufficient heat during plasma coating. The NiCrAlY coating surface has lots of micropores and a few large pores are noticed which would fasten the molten salt penetration into the coating. The EDS results reveal that NiCrAlY coating surface predominantly has Ni, Al and Cr. In case of YSZ coating, Zr is the predominant element along with

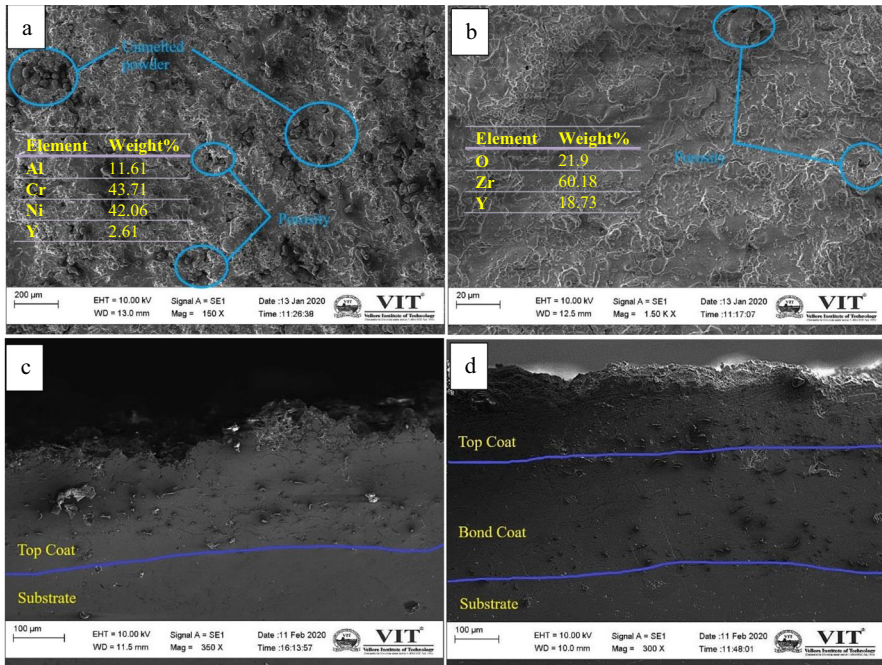


**Fig. 4** SEM surface and cross-sectional microstructure of the **a** and **c** NiCrAlY and **b** and **d** YSZ coating employed by plasma method

minor Y and O are noticed. Figure 4c and d shows the cross-sectional SEM image of plasma-sprayed NiCrAlY and thermal barrier YSZ coating. In the case of NiCrAlY, only one layer of coating is performed which has a lamella structure. The coating shows a dense structure with well-bonded, fewer pores and cracks and thickness was obtained in the range of 165–175  $\mu\text{m}$ . In YSZ coating, two coating layers are formed which are the bond coat is of NiCrAlY and the top-coat is of YSZ. YSZ cannot be directly coated on the selected alloy A-286 due to the variation of CTE value between substrate and YSZ. Both the coatings show the lamella structure with a thickness of 403  $\mu\text{m}$  (BC-300  $\mu\text{m}$  and TC-103  $\mu\text{m}$ ). It is inferred from the SEM analysis that both the coatings have some micropores and there are no cracks and inclusions that could be found in the interface which suggests that the coatings are well bonded with the substrate.

The XRD plots of the coatings (NiCrAlY and YSZ) performed by plasma spray technique are depicted in Fig. 5. It is noticed from the XRD patterns, tetragonal  $\text{ZrO}_2$  phase was seen as the major phase in the YSZ coating. Similarly, in NiCrAlY coating, major phases Ni and  $\text{Ni}_3\text{Al}$  are found and low intensity of peaks Cr and  $\text{Cr}_2\text{O}_3$  is noticed as-sprayed condition which may be attributed to the during solidification of impacting splats or in-flights particles oxidation on the surface.

Microhardness was tested on the cross section of the coated samples and the hardness profile is shown in Fig. 6. The hardness value is around 300–340 HV on the substrate region and the interface region shows the high hardness value than substrate



**Fig. 5** XRD pattern of the plasma-sprayed NiCrAlY and YSZ coating

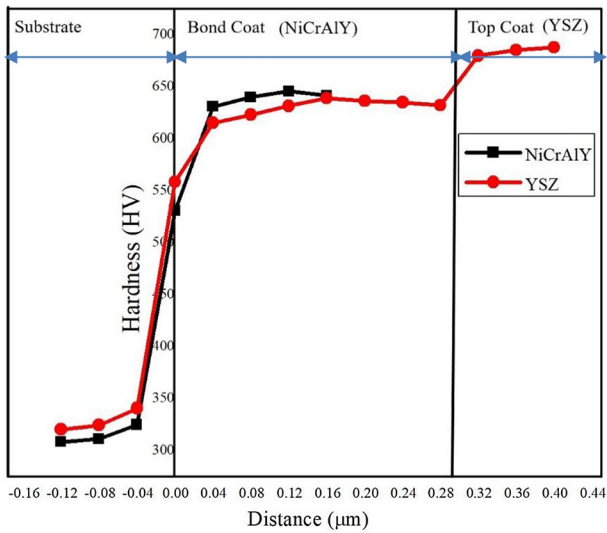
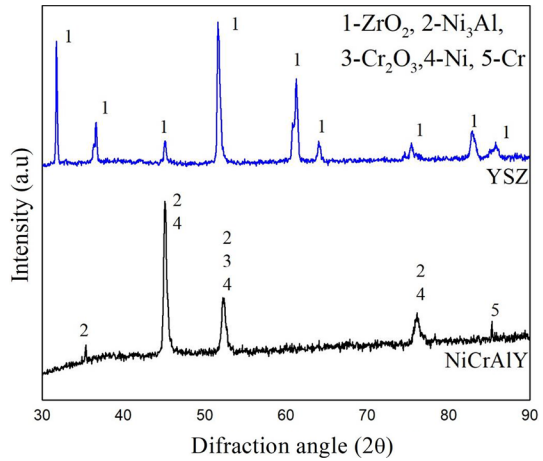


**Fig. 6** Microhardness plot of the plasma-sprayed coating on alloy A-286

is about (515–550 HV) due to shot peening or work hardening effect and the higher kinetic energies of powder particles. NiCrAlY coating region has a hardness value ranging between 600–638 HV and YSZ region has a range of 671–688 HV. It is inferred from the microhardness results, and the coating region has high hardness value than the substrate region due to metallurgical change.

## Hot Corrosion Study

### Visual Analysis and Weight Gain Plot

Figure 7 represents the macro-images of the samples during exposure to the salt environment at 900°C for 10 cycles. During the corrosion study, change in weight

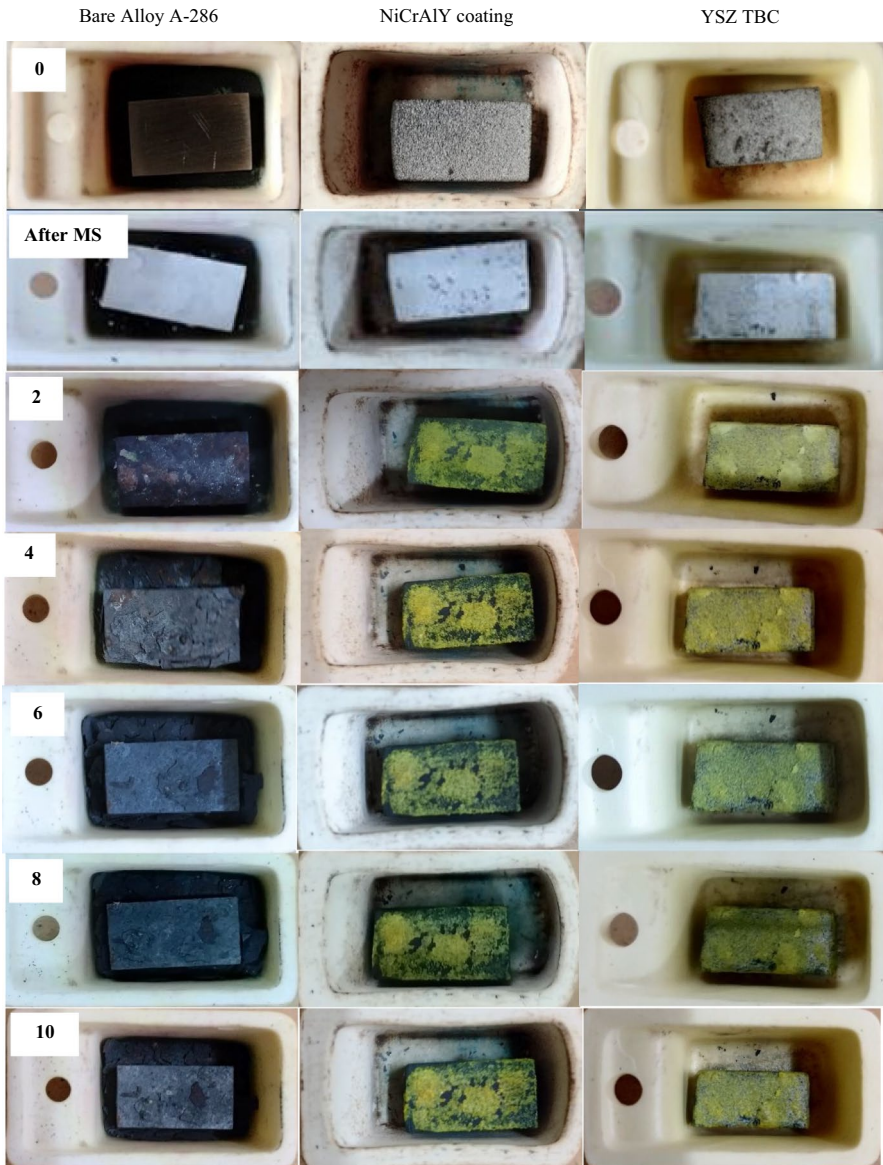


**Fig. 7** Macro-images of the bare, NiCrAlY and YSZ coated alloy A-286 during corrosion study at different cycles

and colour was observed and noted after each cycle. It is observed that the bare sample turned dark black after the first cycle and NiCrAlY and YSZ samples turned yellowish-green. Fragile scales are observed and lots of spallation could be witnessed on the bare specimen which indicates that the non-protective and porous oxide layer formation. The spalled scales were collected in the crucibles till the end of the test and were included during the weight measurement [25, 26]. Whereas in the coated samples, there was no spallation was noticed.

The weight gain curve for the coated and bare alloy A-286 after being exposed to salt conditions is depicted in Fig. 8. The weight gain plot (Fig. 8) shows that the sample coated with YSZ powder shows a high corrosion resistance and less weight gain compared to the sample coated with NiCrAlY powder and uncoated material. The cumulative weight gain and Kp value are listed in Table 3. The Kp value for the uncoated specimen is much higher than the coated specimens which indicates that the high corrosion rate and highly subjected to corrosion.

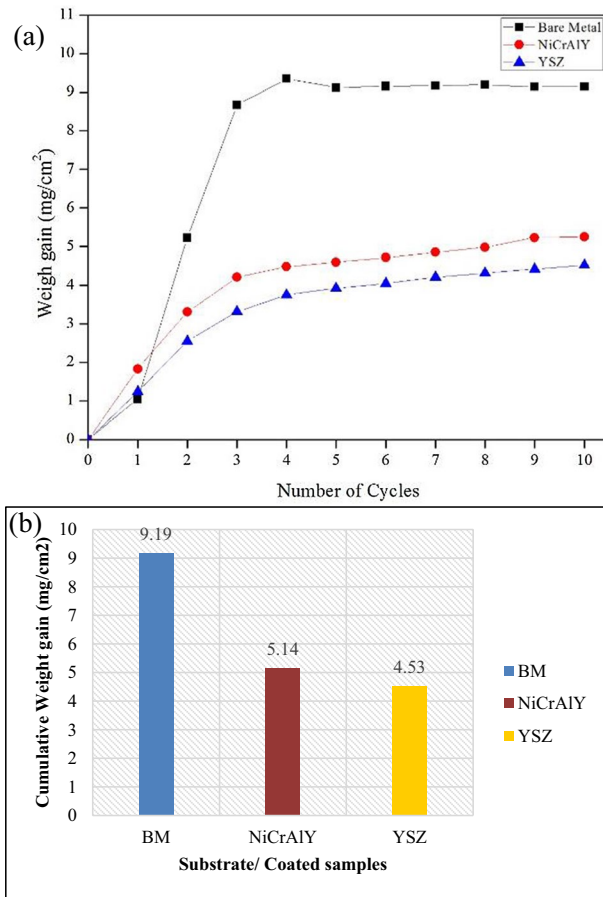


Fig. 8 Weight gain plot and cumulative weight gain histogram of the corroded alloy A-286

**Table 3** Weight gain and  $K_p$  values of the corroded samples

Specimens	Bare specimen	YSZ coating	NiCrAlY coating
Weight gain/unit area ( $\text{mg}/\text{cm}^2$ )	9.1479	4.5264	5.0824
$K_p$ ( $\times 10^{-10} \text{ g}^2\text{cm}^{-4} \text{ s}^{-1}$ )	2.3245	0.5691	0.7175

## Surface Morphology

The surface and compositional analysis of the coated and bare Alloy A-286 after corrosion was observed using SEM and EDS techniques which are presented in Fig. 9. It can be seen that the reaction products fully covered the coating. The scales developed on the uncoated alloy A-286 at 900°C (Fig. 9a) depict the plate and crystalline shape morphology. The EDS results revealed that it has a significant amount of O and Fe along with a little amount of Cr, Ni, Na, S, Cl and V. The SEM morphology of the corroded NiCrAlY coated sample shows the spongy nodular structure as shown in Fig. 9b. The EDS results on the surface show a predominant percentage of Ni and O along with Al, Cr, V, Na, Cl and S. SEM results of YSZ corroded sample surface (Fig. 9c) show the rod and plate-like morphology, and the compositions of the scales were examined by EDS and reported.

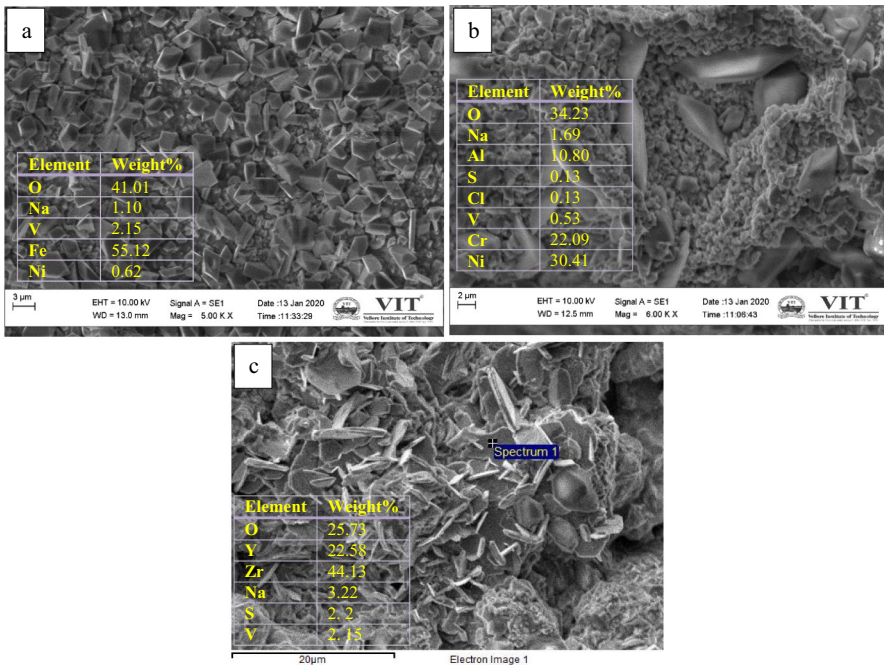


**Fig. 9** SEM–EDS elements analysis of the corroded surface of the **a** Bare **b** NiCrAlY coated and **c** TBC-YSZ coated Alloy A-286

## XRD Analysis on Corrosion Sample

Figure 10 illustrates the XRD analysis of the corroded TBC coated and uncoated alloy A-286. The XRD analysis indicated that  $\text{Fe}_2\text{O}_3$  is the main scale in the case of uncoated specimen along with minor phases such as NiO,  $\text{Cr}_2\text{O}_3$ ,  $\text{NiCr}_2\text{O}_4$ , FeS, NiS and CrS are found. XRD analysis for the NiCrAlY coated A-286 alloy shows the existence of NiO,  $\text{Cr}_2\text{O}_3$ ,  $\text{NiAl}_2\text{O}_4$  and  $\text{NiCr}_2\text{O}_4$  as the predominant phases along with  $\text{Al}_2\text{O}_3$ , NiS,  $\text{YVO}_4$  and CrS phases. In the case of YSZ-coated specimen,  $\text{YVO}_4$  and  $\text{ZrO}_2$  are noticed due to the reaction of  $\text{NaVO}_3$  and YSZ coating.

## Cross Section Study

After corrosion study, the samples are sectioned using a diamond saw cutter for a cross-sectional study. Then, the sectioned side was subjected to mirror finish which is followed by the standard metallographic procedure. The SEM analysis on the uncoated specimen (Fig. 11) shows the oxides developed on the top surface which contains many pores and cracks. A significant amount of O, Fe, Cr and Ni are observed in the scale (Point 1). There is no O found at Points 3 and 4 which suggests that no oxidation. The SEM micrograph for the cross section of corroded NiCrAlY coating (Fig. 12) shows that the coating is well adherent to the substrate and there is no cracks found in the interface region. SEM image indicated that the existence of thin scale in the top region. Point 1 contains the significant level of O, Ni and Cr which suggests the development of NiO and  $\text{Cr}_2\text{O}_3$  scales. O is present in point 1 only which is not observed at points 2 and 3. This indicated that the top surface only is subjected to oxidation. No failures were found in the coating region and also no corrosive elements were noticed in the substrate. From the SEM cross-sectional

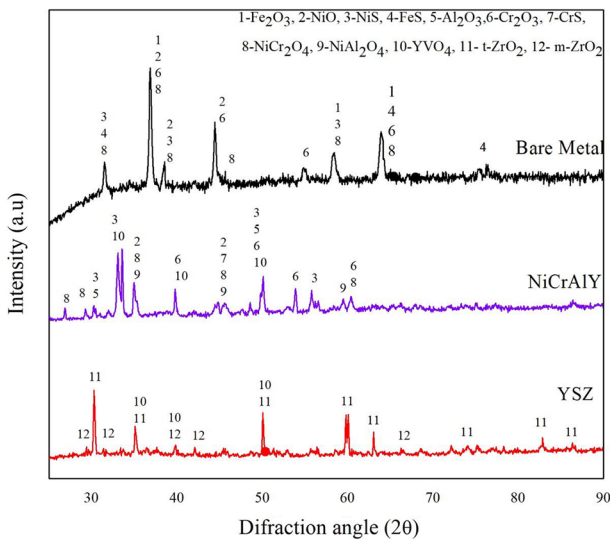


Fig. 10 XRD analysis of the hot corroded alloy A-286

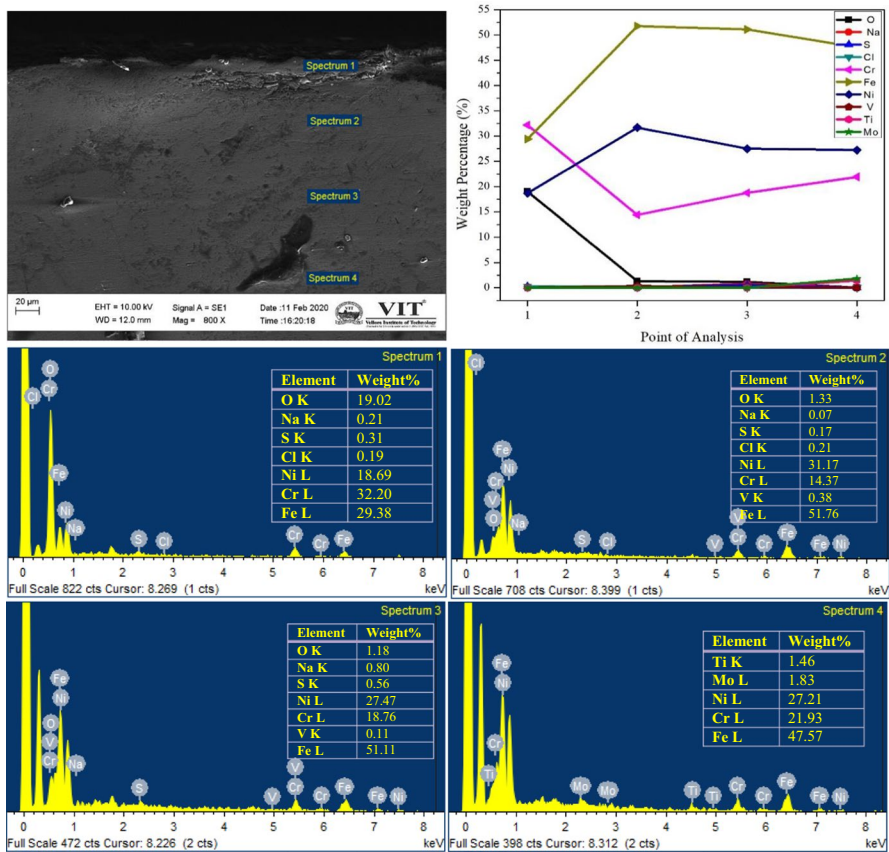


Fig. 11 SEM cross-sectional analysis of the hot corroded uncoated alloy A-286 after corrosion test

examination on the YSZ-coated specimen (Fig. 13), it can be noticed that a thin layer was formed on the top coating and a minor corrosion attack was observed. There was no coating failure and corrosion damage found on the bond coat and good bonding was maintained with top YSZ coating after completion of the corrosion study. The EDS results suggest that the topcoat contains the Y, O and V which indicates the  $YVO_4$  formation.

### Elemental Line Mapping

The EDS line scan investigation on the cross section of the bare metal after corrosion is represented in Fig. 14. It shows the higher composition of O and Fe and also other elements such as Ni and Cr are found at top scale along with corrosion products such as S, Cl, V and Na. A similar trend is seen in EDS line mapping of corroded NiCrAlY and YSZ specimens as shown in Figs. 15 and 16, respectively. In case of NiCrAlY coating (Fig. 15), scales mainly contain O, Ni and Al. This suggests the

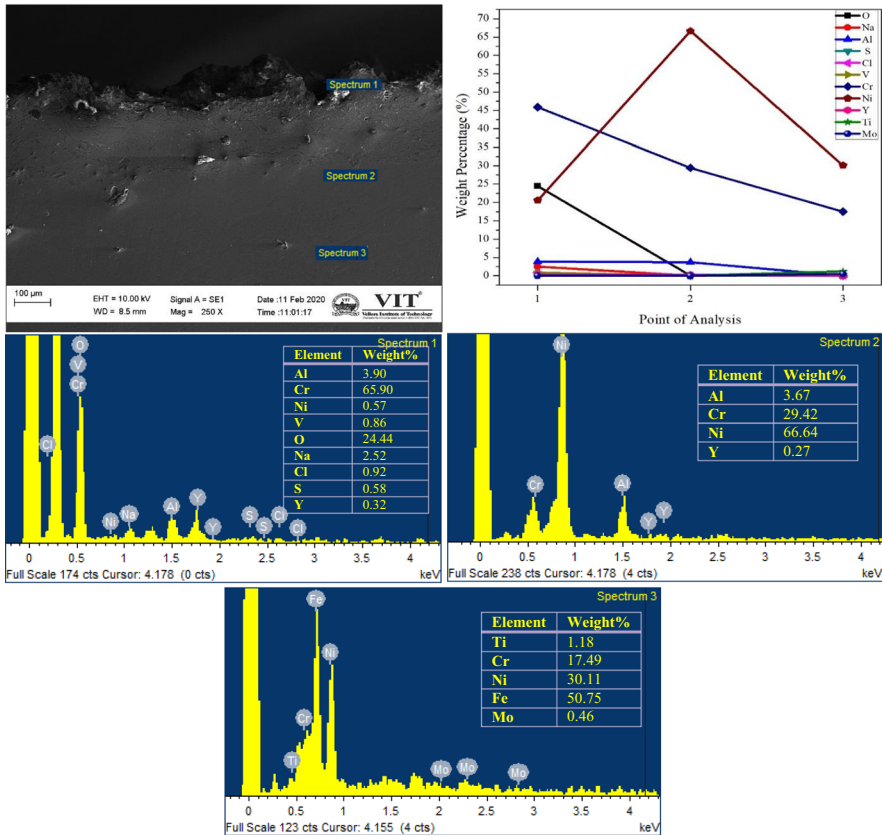
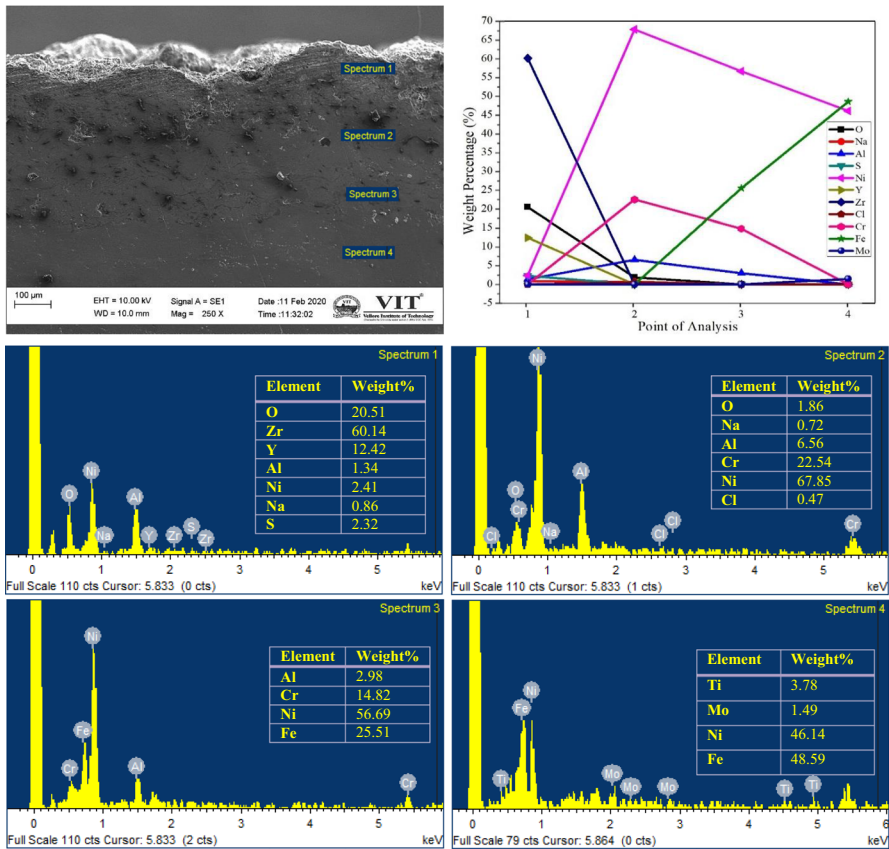


Fig. 12 SEM cross-sectional analysis of the hot corroded NiCrAlY coated alloy A-286 after corrosion test

development of oxides of Ni and Al. The distribution of S and Na decreases and Fe, Ni and Cr increase as we move towards the substrate region from the coating top surface. The scales present on the YSZ coating (Fig. 16) shows the distribution of high O, Zr, Y, V and Na in top scale.

### Discussion

YSZ and NiCrAlY coatings have been deposited successfully on the alloy A-286 with desirable thicknesses of 403 μm and 178 μm using the plasma spraying technique. The surface roughness value was observed to be higher in the case of YSZ coating with an average value of 6.0063 μm than in NiCrAlY coating with an average of 5.8470 μm. It can be seen from the SEM analysis (Fig. 4); few micropores are observed on the coating surface. SEM image of the coated samples clearly depicts that the coatings are dense, uniform and adherent. The XRD analysis was



**Fig. 13** SEM cross-sectional analysis of the hot corroded YSZ coated alloy A-286 after corrosion test

performed on the coatings in order to determine the existed phases. The XRD results (Fig. 5) show that predominant phases are Ni and Ni<sub>3</sub>Al and a minor phase of Cr in NiCrAlY and in YSZ the phases identified mainly are ZrO<sub>2</sub> and Y. In both the case of YSZ and NiCrAlY coatings, the coating region exhibited the high hardness than the substrate due to microstructural features. Microhardness profile (Fig. 6) indicates that an interface between the coating and the substrate shows an increased hardness value than the substrate region because of the shot peening effect of powder particles [3]. The average microhardness values for NiCrAlY and YSZ coatings are 643 HV and 673 HV, respectively.

The corrosion test was done on the coated and uncoated alloy A-286 in a three-salt mixture (3SM) environment. Thermogravimetric analysis (Fig. 8) briefly explains that at the starting cycles, all the samples show a high weight gain because of the oxidation of active elements in the substrate and coating resulting in new oxide layers formation [3, 25]. Subsequently, the weight increase is considerably gradual with the progress in the experiment. The bare metal experiences high weight gain than NiCrAlY coated and YSZ coated samples after the corrosion run. The



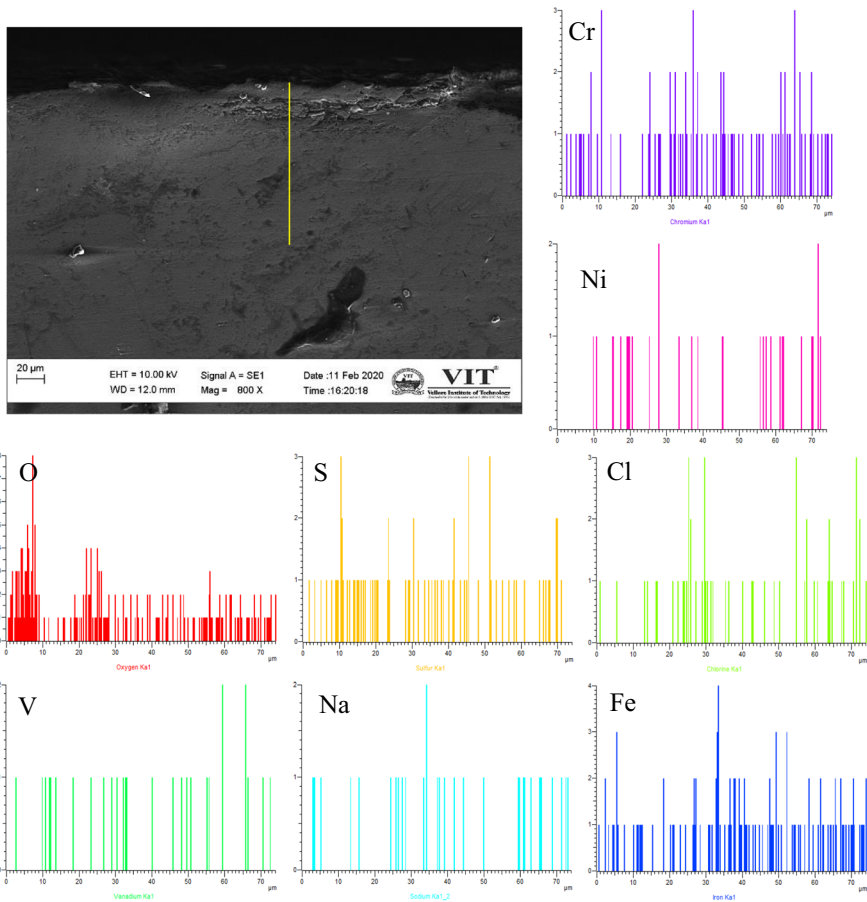


**Fig. 14** Line scan mapping of corroded bare alloy A-286 at cross section

maximum weight gain was obtained on the bare sample and the least was found on the YSZ coating. The  $K_p$  value for bare metal, NiCrAlY and YSZ-coated samples is 2.3245, 0.7175 and 0.5691 ( $\times 10^{-10} \text{ g}^2 \text{ cm}^{-4} \text{ s}^{-1}$ ), respectively. During the corrosion study, the bare metal changed to dark black and shows major spallation. An important observation made from the study is, bare metal showed high weight gain up to the 4th cycle, later weight gain is levelled off due to spallation. It is inferred from the results that the bare metal was severely susceptible to corrosion attack resulted in scales sputtering and spallation at the elevated temperature due to non-protective  $\text{Fe}_2\text{O}_3$  scale formation [26, 27]. A porous and loose scales were developed on the surface which was easily peeled off during cooling due to thermal stress. Sidhu et al. [27] reported that high weight gain in alloy 800H and it was subjected to severe sputtering and peeling of scales during the exposure to  $\text{Na}_2\text{SO}_4$ -60%  $\text{V}_2\text{O}_5$  environment. High strain and stress could be induced in the scales due to precipitation of  $\text{Fe}_2\text{O}_3$  during cooling.  $\text{Fe}_2\text{O}_3$  is porous in nature which allows the O and other

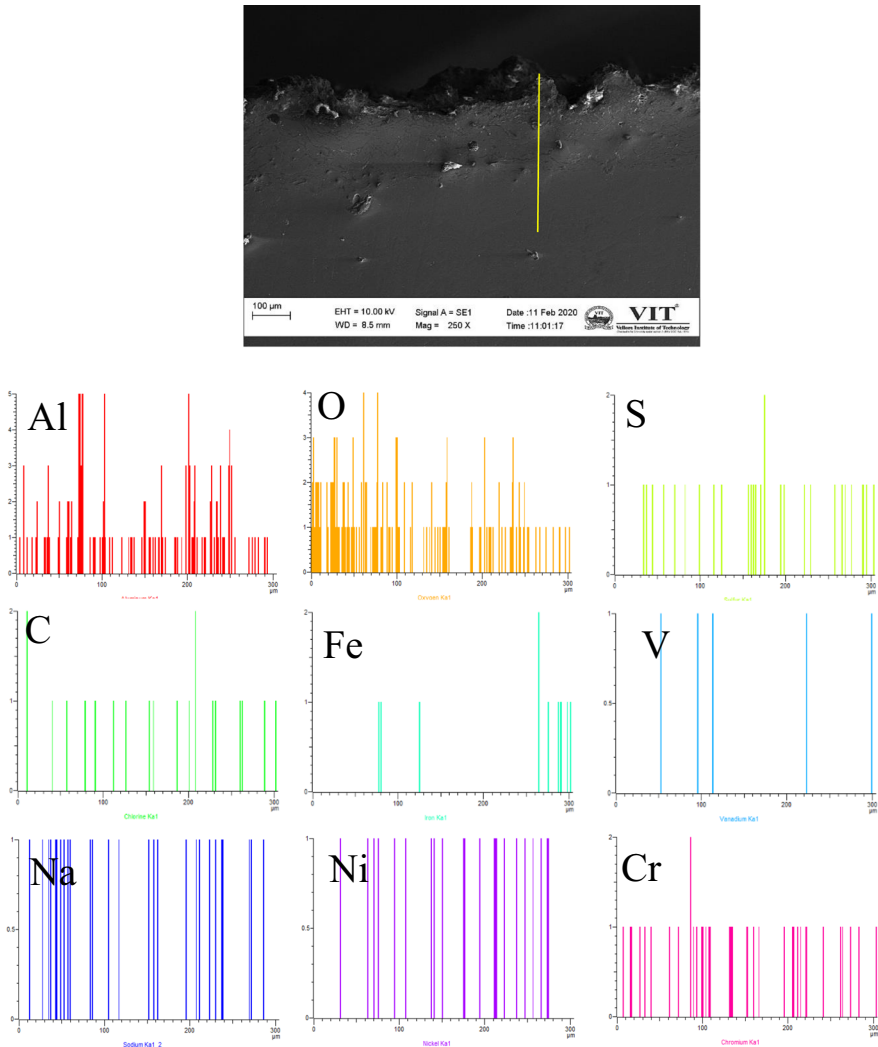


**Fig. 15** Line scan mapping of corroded NiCrAlY coated alloy A-286 at cross section

corrosive species to react with the substrate material directly due to this more oxidation takes place on the surface and causes the development of thick scale. Thermal expansion value for the scales developed on the surface of the specimen also plays a significant role in the crack formation and spallation [6, 26]. The spalling rate of scales from the sample is observed from 1st cycle onwards and the rate of spalling increased with an increase in time which is clearly depicted by macro-images [27]. The value of the parabolic rate constant ( $K_p$ ) and weight gain for the uncoated specimen is  $2.3245 \times 10^{-10} \text{ g}^2\text{cm}^{-4} \text{ s}^{-1}$ . The loose and fragile  $\text{Fe}_2\text{O}_3$  scales were mainly developed on the uncoated sample. The EDS and XRD analysis confirmed that the

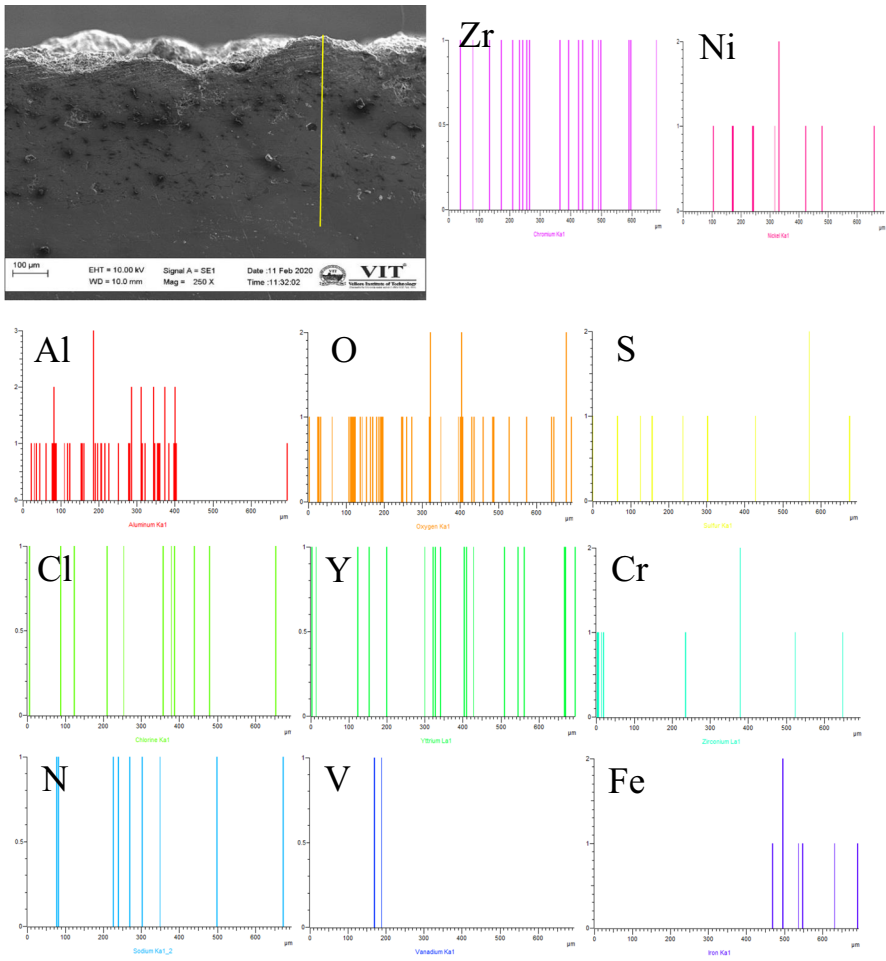
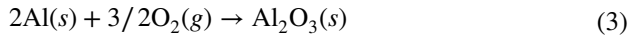
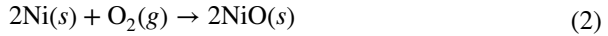
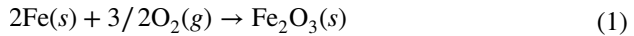


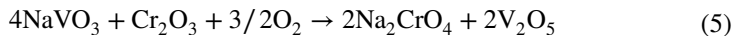
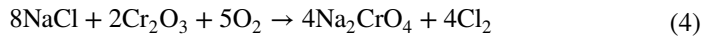
**Fig. 16** Line scan mapping of corroded YSZ TBC at cross section

existence of other phases such as NiO, NiCr<sub>2</sub>O<sub>4</sub>, Cr<sub>2</sub>O<sub>3</sub>, NiS, FeS and CrS in the uncoated specimen. The reaction of metal oxide formation is explained by Eqs. (1–3) [3, 6]. This might be concluded by the presence of elements such as Ni and Cr in the substrate getting oxidized and also the reaction of sulphur from Na<sub>2</sub>SO<sub>4</sub> during the exposure. The presence of metal sulphides in the scales suggests that the uncoated specimen experienced sulphidation [6, 28]. The cross-sectional study inferred that the oxide scales in the uncoated specimen are thin and porous Fe<sub>2</sub>O<sub>3</sub> scales which is confirmed by EDS point and line mapping technique along the cross section. Due to more spallation, a thin layer of scales was noticed and the corrosion products were distributed upto 70 μm. The point EDS inspection at cross section shows the presence of the corrosion end results such as O, S, Fe, Na and Cl which is additionally backed up by X-ray line mapping. The existence of these corrosive

species decreases with increasing the depth of analysis from the top surface of the substrate.



The presence of  $\text{NaVO}_3$  (m.p 610 °C) in the environment attributes the high oxidation, which acts as oxygen carries and stimulant to the material and results in high weight gain as found in the uncoated specimen. The  $\text{NaCl}$  (m.p 801°C) and  $\text{NaVO}_3$  salts react with chromium oxide to form sodium chromate thereby releasing volatile chlorine as governed by Eqs. (4 and 5). The formed  $\text{Na}_2\text{CrO}_4$  evaporated as a gas [28–31].

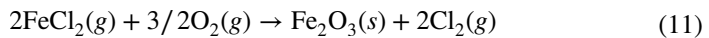


In the case of coated specimens, weight gain is high till 3rd cycle after that drastically weight drop was observed and also no spallation could be found till the end of the experimentation. This was attributed to the diffusion of O and other reactive elements restricted by the development of protective  $\text{NiO}$ ,  $\text{Al}_2\text{O}_3$ ,  $\text{Cr}_2\text{O}_3$  scales in the  $\text{NiCrAlY}$  coating and  $\text{ZrO}_2$  in the  $\text{YSZ}$  coating. The stable spinel oxides  $\text{NiCr}_2\text{O}_4$  and  $\text{NiAl}_2\text{O}_4$  could form in the coated specimen which prevents the salt penetration and provides the corrosion resistance in the salt condition and the reaction was explained by Eqs. (6 and 7) [16]. The cross section SEM investigation of the corroded  $\text{NiCrAlY}$  coated sample (Fig. 12) shows the dense layer of scale and the absence of corrosion product in the substrate region which is supported by EDS results. Elemental mapping (Fig. 15) also proves the absence of corrosion products in the substrate region. A minor composition of Fe is found in the coating region which is the result of thermal diffusion from the substrate. The protective stable scales were noticed on the  $\text{NiCrAlY}$  coated sample which acts as diffusion barrier of O and other corrosive elements and slows down the oxidation process resulting in minimal weight gain was achieved than bare alloy.



Further, the presence of corrosive Cl in the environment would dissolve the scale above 400°C and result in cracks development on the scales. The specimens were experienced to active oxidation in the presence of Cl medium. The degradation rate was increased with increasing the temperature and time. Through these cracks and pores, the O and Cl could penetrate into the scales and coatings and

it comes in contact with the elements resulting in the development of metal chlorides that are porous and volatile in nature. These porous layers allow the O causing oxides would form and increase the rate of oxidation. This oxy-chlorination is reported in Eqs. (8–11) [6, 29].



The YSZ coating exhibits minimum weight gain out of all samples. This shows that YSZ coating is better corrosion resistance than the bare and NiCrAlY-coated sample. The yellow patches indicate the deposited salts.



The deposited  $\text{NaVO}_3$  (m.p  $610^\circ\text{C}$ ) is liquid state salt that reacts with  $\text{Y}_2\text{O}_3$  in the ceramic topcoat YSZ lead to the development of the tetragonal  $\text{ZrO}_2$  phase which is stable up to  $1200^\circ\text{C}$ . It is explained by Eq. (12). Then, the phase transformation occurred from the tetragonal to monoclinic  $\text{ZrO}_2$  phase. The entire surface of the corroded YSZ TBC coating (Fig. 9) was covered by rod-like  $\text{YVO}_4$  scale along with  $m\text{-ZrO}_2$  ( $m$  refers monoclinic) after the corrosion run which contributes to the YSZ topcoat deterioration [30, 31]. There is no corrosion damage which is found in the BC region and also good adherence was obtained between the YSZ and NiCrAlY. The high porosity in the topcoat leads to salt penetration into the coating and degradation more [32]. But in our case, the less porosity in the YSZ top coating block the O and corrosive salts penetration by developing the thin  $\text{ZrO}_2$  layer. The XRD results confirm that the existence of  $\text{YVO}_4$ , tetragonal  $\text{ZrO}_2$  and monoclinic  $\text{ZrO}_2$  phases on the corroded surface of the YSZ coating [33–37]. This is supported by cross section EDS and X-ray line mapping (Fig. 16) which proves the absence of corrosion products at the interface and substrate region. It can be noticed that the corrosion depth is very low for YSZ-coated samples than other samples. The hot corrosion mechanism of the alloy A-286 is illustrated in Fig. 17 which clearly indicates that the scales formation and failure.

The hot corrosion mechanisms involved in the TBC system is emphasized by the following steps,

- i. Molten salt penetration through cracks and open pores in the ceramic top coat.
- ii. Corrosive molten salt reaction with stabilizer zirconia ( $\text{Y}_2\text{O}_3$ ,  $\text{ZrO}_2$ )
- iii. Owing to the depletion of the zirconia stabilizer, the phase of the zirconia was transformed from tetragonal to monoclinic.
- iv. Rod shape  $\text{YVO}_4$  crystal formation was obtained by reaction of  $\text{NaVO}_3$  and YSZ.

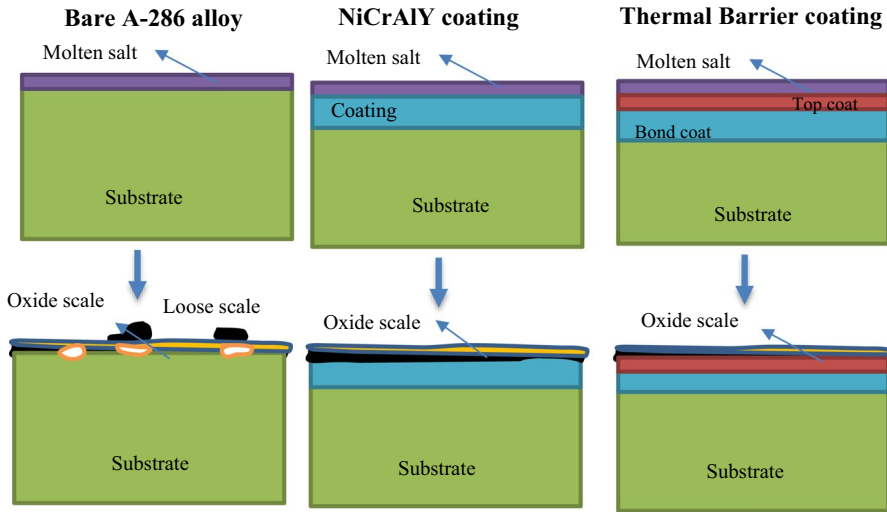


Fig. 17 Schematic diagram of corrosion mechanism of the bare and coated alloy A-286

## Conclusions

The NiCrAlY and TBC YSZ coatings were successfully deposited on the alloy A-286 using plasma spray process to perform under harsh environment and the following conclusions were summarized on the corrosion behaviour of the bare and coated alloy in 3SM environments at 900°C.

1. The thickness of the coatings such as NiCrAlY and YSZ was achieved in the range of 178 and 403  $\mu\text{m}$  and the coating is well bonded to the substrate and there are no defects found in the interface.
2. The bare sample was more prone to corrosion attack due to the direct reaction of salt and the substrate and resulted in rapid formation of porous and loose  $\text{Fe}_2\text{O}_3$  scale. Besides, the existence of S and Cl also enhances the rate of oxidation and damaged the scales more resulted in more scales spallation.
3. The weight gain per unit area due to spallation was 9.147  $\text{mg}/\text{cm}^2$  for bare metal, 4.526  $\text{mg}/\text{cm}^2$  for YSZ-coated samples and 5.082  $\text{mg}/\text{cm}^2$  for NiCrAlY coated samples. The YSZ and NiCrAlY samples have shown 50.52% and 44.45% lesser weight gain than the bare metal samples, respectively.
4. YSZ-coated sample exhibits high resistance to corrosion than the bare and NiCrAlY coated samples due to the development of dense and adherent monoclinic  $\text{ZrO}_2$  scales and both coatings show superior resistance to corrosion and spallation due to the development of different oxide of Cr, Al and Ni.

**Acknowledgements** The authors would also like to thank Lab in charges of Materials Engineering Technology Laboratory and Advance Materials processing laboratory, VIT-Vellore for providing all the facilities to carry out the research work.

**Author contributions** SMM was involved in Conceptualization, Methodology, Investigation, Writing—original draft; MA contributed to Methodology, Investigation; CJ was involved in review & editing; SV contributed to Investigation, Writing—review & editing. KSP was involved in Writing—review & editing, Validation. MV contributed to Supervision, Writing—review & editing. VDVS was involved in review & editing; NA contributed to Writing—review & editing.

## Declarations

**Conflict of interest** The authors have no conflict of interest.

## References

1. Ó. Martín, P. De Tiedra, and M. San-Juan, *Materials Science and Engineering: A* **688**, 2017 (309–314).
2. O. O. Tinubu, S. Das, A. Dutt, J. E. Mogonye, V. Ageh, R. Xu, J. Forsdike, R. S. Mishra, and T. W. Scharf, *Wear* **356**, 2016 (94–100).
3. S. M. Muthu and M. Arivarasu, *Engineering Failure Analysis* **107**, 2020 (104224).
4. D. Kumar and V. K. Dwivedi, *Advances in Materials and Processing Technologies* **9**, (2), 2023 (536–550).
5. N. Eliaz, G. Shemesh, and R. M. Latanision, *Engineering Failure Analysis* **9**, (1), 2002 (31–43).
6. S. M. Muthu and M. Arivarasu, *Surface Topography: Metrology and Properties*. **8**, (4), 2020 (045021).
7. B. Wei, C. Chen, J. Xu, L. Yang, Y. Jia, Y. Du, M. Guo, C. Sun, Z. Wang, and F. Wang, *Corrosion Science*. **195**, 2021 (109996).
8. D. Kumar, *Transactions of the Indian Institute of Metals* **72**, (7), 2019 (1927–1939).
9. N. P. Padture, M. Gell, and E. H. Jordan, *Science* **296**, (5566), 2002 (280–284).
10. M. H. Habibi and S. M. Guo, *Materials and Corrosion* **66**, (3), 2015 (270–277).
11. D. E. Mack, M. Tandler, Y. J. Sohn, D. Sebold, and O. Guillon, *Journal of the American Ceramic Society* **104**, (1), 2021 (463–471).
12. D. Kumar and K. Npandey, *Sadhana* **46**, 2021 (1–17).
13. I. N. Qureshi, M. Shahid, and A. N. Khan, *Journal of Thermal Spray Technology* **25**, (3), 2016 (567–579).
14. D. R. Clarke, M. Oechsner, and N. P. Padture, *MRS Bulletin* **37**, (10), 2012 (891–898).
15. B. Guerreiro, R. S. Lima, N. Curry, M. Leitner, and K. Körner, *Journal of Thermal Spray Technology* **30**, (1), 2021 (59–68).
16. P. Shi, W. Wang, S. Wan, Q. Gao, H. Sun, X. Feng, G. Yi, E. Xie, and Q. Wang, *Surface and Coatings Technology* **405**, 2021 (126615).
17. G. Singh, K. Goyal, and R. Goyal, *Universal Journal of Mechanical Engineering* **7**, 2019 (247–254).
18. L. Guo, H. Xin, Z. Zhang, X. Zhang, and F. Ye, *Journal of Advanced Ceramics* **9**, (2), 2020 (9).
19. J. Shi, T. Zhang, B. Sun, B. Wang, X. Zhang, and L. Song, *Journal of Alloys and Compounds* **844**, 2020 (156093).
20. P. G. Lashmi, P. V. Ananthapadmanabhan, G. Unnikrishnan, and S. T. Aruna, *Journal of the European Ceramic Society* **40**, (8), 2020 (2731–2745).
21. S. K. Essa, K. Chen, R. Liu, X. Wu, and M. X. Yao, *Journal of the European Ceramic Society* **30**, (1), 2021 (424–441).
22. S. Xie, C. Song, Z. Yu, S. Liu, F. Lapostolle, D. Klein, C. Deng, M. Liu, and H. Liao, *Journal of the European Ceramic Society* **41**, (1), 2021 (535–543).
23. M. S. Ahmadi, R. Shoja-Razavi, Z. Valefi, and H. Jamali, *Optics and Laser Technology* **111**, 2019 (687–695).
24. D. Kumar, K. N. Pandey, and D. K. Das, *Proceedings of the Institution of Mechanical Engineers Part L: Journal of Materials: Design and Applications* **232**, (7), 2018 (582–591).
25. D. Kumar and K. N. Pandey, *Metals and Materials International* **27**, 2021 (5322–5334).
26. S. M. Muthu, M. Arivarasu, and N. Arivazhagan, *Procedia Structural Integrity* **14**, 2019 (290–303).
27. T. S. Sidhu, S. Prakash, and R. D. Agrawal, *Acta Materialia* **54**, (3), 2006 (773–784).

28. D. Kumar and K. N. Pandey, *International Journal of Mechanical and Production Engineering* **2**, 2014 (19–22).
29. W. Zhou, K. Zhou, C. Deng, K. Zeng, and Y. Li, *Ceramics International* **43**, (12), 2017 (9390–9400).
30. S. M. Muthu and M. Arivarasu, *Transactions of the Indian Institute of Metals* **72**, 2019 (1607–1612).
31. P. K. Koech and C. J. Wang, *Oxidation of Metals* **90**, (5–6), 2018 (713–735).
32. X. Zhong, Y. Wang, Z. Xu, Y. Zhang, J. Zhang, and X. Cao, *Materials Corrosion* **60**, (11), 2009 (882–888).
33. R. Ahmadi-Pidani, R. Shoja-Razavi, R. Mozafarinia, and H. Jamali, *Ceramics International* **38**, (8), 2012 (6613–6620).
34. Z. Chen, S. Speakman, J. Howe, H. Wang, W. Porter, and R. Trice, *Journal of the European Ceramic Society* **29**, (8), 2009 (1403–1411).
35. H. Vakiliifard, R. Ghasemi, and M. Rahimipour, *Surface and Coatings Technology* **326**, 2017 (238–246).
36. D. Kumar, *Indian Journal of Chemical Technology (IJCT)* **24**, (2), 2017 (153–161).
37. S. Wu, Y. Zhao, W. Li, W. Liu, Y. Wu, and Z. Zhao, *Journal of Thermal Analysis and Calorimetry* **144**, (6), 2021 (2043–2056).

**Publisher's Note** Springer Nature remains neutral with regard to jurisdictional claims in published maps and institutional affiliations.

Springer Nature or its licensor (e.g. a society or other partner) holds exclusive rights to this article under a publishing agreement with the author(s) or other rightsholder(s); author self-archiving of the accepted manuscript version of this article is solely governed by the terms of such publishing agreement and applicable law.

## Authors and Affiliations

**S. M. Muthu<sup>1</sup> · M. Arivarasu<sup>2</sup> · Changheui Jang<sup>1</sup> · S. Viknesh<sup>3</sup> ·  
K. Surya Prakash Reddy<sup>4</sup> · M. Venkateshkannan<sup>5</sup> · V. D. Vishnu Siddharth<sup>4</sup> ·  
Nafeez Ahmed Liyakat<sup>6</sup>**

✉ S. M. Muthu  
muthumech1992@gmail.com

<sup>1</sup> Department of Nuclear and Quantum Engineering, Korea Advanced Institute of Science and Technology, Daejeon 34141, Republic of Korea

<sup>2</sup> Centre for Innovative Manufacturing Research, Vellore Institute of Technology, Vellore 632014, India

<sup>3</sup> Faculty of Mechanical Engineering, University of Technology Chemnitz, 09107 Chemnitz, Germany

<sup>4</sup> School of Mechanical Engineering, Vellore Institute of Technology, Vellore 632014, India

<sup>5</sup> School of Engineering and Technology, Dhanalakshmi Srinivasan University, Trichy 621112, India

<sup>6</sup> Department of Mechanical and Automation Engineering, Gojan School of Business and Technology, Chennai 600052, India